ISSN 1070-3284, Russian Journal of Coordination Chemistry, 2023, Vol. 49, No. 3, pp. 148–157. © Pleiades Publishing, Ltd., 2023.
Russian Text © The Author(s), 2023, published in Koordinatsionnaya Khimiya, 2023, Vol. 49, No. 3, pp. 163–173.

Cu(II), Ni(II), Co(II), Zn(II), and Pd(II) Complexes with (4*Z*)-4-[(2-Furylmethylamino)methylene]-5-methyl-2-phenylpyrazol-3-one: Synthesis, Structures, and Properties

V. G. Vlasenko[a], *, A. S. Burlov[b], M. S. Milutka[b], Yu. V. Koshchienko[b], A. I. Uraev[b], V. A. Lazarenko[c], N. I. Makarova[b], A. V. Metelitsa[b], A. A. Zubenko[d], and D. A. Garnovskii[e]

[a] *Institute of Physics, Southern Federal University, Rostov-on-Don, Russia*
[b] *Institute of Physical and Organic Chemistry, Southern Federal University, Rostov-on-Don, Russia*
[c] *National Research Center Kurchatov Institute, Moscow, Russia*
[d] *North Caucasian Zonal Scientific Research Veterinary Institute, Novocherkassk, Russia*
[e] *Southern Scientific Center, Russian Academy of Sciences, Rostov-on-Don, Russia*
**e-mail: v_vlasenko@rambler.ru*

Received June 10, 2022; revised August 25, 2022; accepted August 31, 2022

Abstract—(4*Z*)-4-[(2-Furylmethylamino)methylene]-5-methyl-2-phenylpyrazol-3-one (HL) and its Cu(II), Ni(II), Co(II), Zn(II), and Pd(II) complexes with the ML_2 composition are synthesized. The structures of the complexes are studied by elemental C,H,N analysis, IR spectroscopy, magnetochemical measurements, and quantum chemistry. The crystal structures of the copper(II) and cobalt(II) complexes are determined by X-ray diffraction (XRD) (CIF files CCDC nos. 2177619 and 2177622, respectively). Two deprotonated ligands are coordinated to the metal ions via the chelate mode by the nitrogen atom of the imino group and the oxygen atom of the hydroxy group of the ligand. The geometry of the copper(II) ion environment corresponds to a distorted planar square, whereas the cobalt(II) ion exists in a distorted tetrahedral environment. In the series of the compounds studied, fluorescence with a maximum at 431 nm and a quantum yield of 0.29 is observed for the Zn(II) complex in a solution of CH_2Cl_2. The synthesized enamine and metal complexes are tested for antibacterial, protistocidal, and fungistatic activities. All compounds are shown to have no fungistatic and antibacterial activities, and only a weak protistocidal activity is found for the copper and zinc complexes.

Keywords: enamines, metallochelates, IR spectroscopy, ^{1}H NMR, UV, photoluminescence, XRD
DOI: 10.1134/S1070328422700221

INTRODUCTION

Pyrazole derivatives represent a huge class of compounds, which are objects of vast research to the present time [1–10]. Emphasis on these compounds is primarily due to their practical significance for medicine, veterinary, and agriculture, since they manifest diverse biological activity. The pyrazole derivatives have antipyretic and analgesic properties [11–13], can exert anticancer [14, 15], antibacterial [16], and antimicrobial [17] effects, and are components of certified drugs (for example, Celebrex®, Viagra®).

The use of the metal complexes based on the pyrazole derivatives as luminescent materials is known along with biological and pharmaceutical applications. The synthesis of new compounds emitting in the blue spectral range and having a set of characteristics (monochromaticity, high photostability, high brightness, and others) for their use as active emitting layers in OLED remains to be an important topical problem. The zinc complexes with the pyrazole-containing ligands that demonstrated high brightness and luminescence efficiency as emitters in OLED were synthesized for this purpose [18–23]. There are recent examples of manufacturing OLEDs based on the rare-earth elements with the pyrazole-containing ligands and emitting in the IR spectral range [24].

The synthetic manipulation and functionalization of the pyrazole framework favor the preparation of numerous coordination nodes of various types [25–27], which makes it possible to monitor changes in many physicochemical properties of these compounds depending on their composition and structure.

For this purpose, continuing our previous studies of the structures and spectral and biological properties of the transition metal complexes [1–10, 28–31], in this work we report the synthesis, crystal structures, and spectral properties of the new pyrazole-containing Schiff base (4*Z*)-4-[(2-furylmethylamino)methy-

lene]-5-methyl-2-phenylpyrazol-3-one (HL) and the Cu (**Ia**), Ni (**Ib**), Co (**Ic**), Zn (**Id**), and Pd (**Ie**) complexes with this ligand. The synthesized compounds were also studied for antibacterial, protistocidal, and fungistatic activities.

EXPERIMENTAL

Commercially available solvents (benzene, methanol, dichloromethane), 2-(aminomethyl)furan (≥99%), copper acetate monohydrate (≥98%), nickel acetate tetrahydrate (98%), cobalt acetate tetrahydrate (≥98%), zinc acetate dihydrate (≥98%), and palladium acetate (98%) (Alfa Aesar) were used as received. 5-Hydroxy-3-methyl-1-phenylpyrazole-4-carbaldehyde was synthesized using published procedures [32, 33].

Synthesis of HL. A solution of 2-(aminomethyl)furan (0.97 g, 10 mmol) in benzene (10 mL) was added to a solution of 5-hydroxy-3-methyl-1-phenylpyrazole-4-carbaldehyde (2.02 g, 10 mmol) in benzene (10 mL). The mixture was refluxed using the Dean–Stark trap for 2 h to the complete separation of water and cooled, and methanol (5 mL) was added. The formed precipitate of HL was filtered off and recrystallized from a methanol–dichloromethane (2 : 1) mixture. The yield of a white powder of HL was 2.40 g (87%).

For $C_{16}H_{15}N_3O_2$

Anal. calcd., %	C, 68.31	H, 5.37	N, 14.94
Found, %	C, 68.39	H, 5.39	N, 15.02

IR (ν, cm^{-1}): 3219 (NH), 3160 (CH_2 of methylfuran), 1681, 1667 (C=O), 1633, 1621, 1595, 1538, 1500, 1486, 1462, 1432, 1366, 1353, 1338, 1305, 1279, 1264, 1202, 1158, 1117, 1082, 1009, 991, 920, 820, 791, 757, 744, 694, 665, 625, 597, 567. ^{1}H NMR (DMSO-d_6; δ, ppm): 2.17 (s, 3H, CH_3), 4.67 (d, J = 5.1 Hz, 2H, CH_2), 6.42 (d, J = 3.0 Hz, 1H, H^3_{furyl}), 6.46 (t, J = 2.4 Hz, 1H, H^4_{furyl}), 7.08 (t, J = 7.4 Hz, 1H, H^4_{phenyl}), 7.35 (t, J = 7.8 Hz, 2H, H^3 and H^5_{phenyl}), 7.68 (s, 1H, H^5_{furyl}), 7.97 (d, J = 7.8 Hz, 2H, H^2 and H^6_{phenyl}), 8.10 (d, J = 13.8 Hz, 1H, CH–NH), 9.74–9.78 (m, 1H, CH–NH).

Synthesis of complexes Ia–Ie. The following solutions were added to a solution of ligand HL (0.56 g, 2 mmol) in a mixture of methanol (10 mL) and dichloromethane (5 mL): copper acetate monohydrate (0.20 g, 1 mmol), nickel acetate tetrahydrate (0.25 g, 1 mmol), cobalt acetate tetrahydrate (0.25 g, 1 mmol), zinc acetate dihydrate (0.22 g, 1 mmol), and palladium acetate (0.25 g, 1 mmol), respectively, in methanol (10 mL). The mixture was refluxed for 2 h. Precipitates of the complexes formed upon cooling were filtered off, washed with methanol, recrystallized from a methanol–dichloromethane (2 : 1) mixture, and dried in a vacuum drying box at 100°C.

Crystals of the complexes suitable for XRD were grown from a methanol–dichloromethane (2 : 1) mixture.

Bis{[4-[(*E*)-2-furylmethyliminomethyl]-5-methyl-2-phenylpyrazol-3-yl]oxy}copper(II) (**Ia**). The yield of brown crystals of compound **Ia** with T_m = 225–226°C was 0.50 g (81%).

For $C_{32}H_{28}N_6O_4Cu$

Anal. calcd., %	C, 61.58	H, 4.52	N, 13.47	Cu, 10.18
Found, %	C, 61.62	H, 4.59	N, 13.51	Cu, 10.25

IR (ν, cm^{-1}): 3140 (CH_2 of methylfuran), 1626 (CH=N), 1596, 1543, 1525, 1502, 1491, 1458, 1441, 1399, 1374, 1333, 1256, 1219, 1188, 1147, 1120, 1091, 1031, 1012, 905, 883, 816, 758, 734, 696, 650, 613, 597. μ_{eff} = 2.10 μ_B (294 K).

Bis{[4-[(*E*)-2-furylmethyliminomethyl]-5-methyl-2-phenylpyrazol-3-yl]oxy}nickel(II) (**Ib**). The yield of green crystals of compound **Ib** with T_m = 155–156°C was 0.47 g (76%).

For $C_{32}H_{28}N_6O_4Ni$

Anal. calcd., %	C, 61.06	H, 4.56	N, 13.57	Ni, 9.48
Found, %	C, 61.11	H, 4.62	N, 13.69	Ni, 9.54

IR (ν, cm^{-1}): 3145 (CH_2 of methylfuran), 1633 (CH=N), 1598, 1549, 1531, 1504, 1465, 1374, 1315, 1183, 1148, 1087, 1013, 900, 821, 757, 731, 693, 623. μ_{eff} = 3.12 μ_B (294 K).

Bis{[4-[(*E*)-2-furylmethyliminomethyl]-5-methyl-2-phenylpyrazol-3-yl]oxy}cobalt(II) (**Ic**). The yield of red-brown crystals of compound **Ic** with T_m = 201–202°C was 0.50 g (81%).

For $C_{32}H_{28}N_6O_4Co$

Anal. calcd., %	C, 62.04	H, 4.56	N, 13.57	Co, 9.51
Found, %	C, 62.17	H, 4.61	N, 13.50	Co, 9.60

IR (ν, cm^{-1}): 3144 (CH_2 of methylfuran), 1621 (CH=N), 1596, 1586, 1531, 1501, 1456, 1372, 1260, 1190, 1145, 1120, 1034, 1011, 1003, 908, 885, 812, 753, 738, 693, 649, 612, 600, 567. μ_{eff} = 4.26 μ_B (294 K).

Bis{[4-[(*E*)-2-furylmethyliminomethyl]-5-methyl-2-phenylpyrazol-3-yl]oxy}zinc(II) (**Id**). The yield of white crystals of compound **Id** with T_m > 300°C was 0.54 g (86%).

For $C_{32}H_{28}N_6O_4Zn$

Anal. calcd., %	C, 61.40	H, 4.51	N, 13.43	Zn, 10.44
Found, %	C, 61.48	H, 4.59	N, 13.50	Zn, 10.52

IR (ν, cm^{-1}): 3111 (CH_2 of methylfuran), 1633 (CH=N), 1620, 1597, 1584, 1500, 1489, 1456, 1388, 1371, 1329, 1264, 1178, 1170, 1147, 1115, 1095, 1018, 974, 957, 901, 813, 756, 736, 721, 694, 611, 597. ^{1}H NMR (DMSO-d_6; δ, ppm): 2.24 (s, 3H, CH_3), 4.50 (s, 2H, CH_2), 6.10 (d, J = 3.3 Hz, 1H, H^3_{furyl}), 6.17 (t, J = 2.6 Hz, 1H, H^4_{furyl}), 7.13 (t, J = 7.4 Hz, 1H, H^4_{phenyl}), 7.33–7.38 (m, 3H, H^3 and H^5_{phenyl}, H^5_{furyl}), 7.78 (d, J = 7.5 Hz, 2H, H^2 and H^6_{phenyl}), 8.36 (s, 1H, CH=N).

Bis{[4-[(*E*)-2-furylmethyliminomethyl]-5-methyl-2-phenylpyrazol-3-yl]oxy}palladium(II) (**Ie**). The yield of a light brown powder of compound **Ie** with T_m > 300°C was 0.55 g (82%).

For $C_{32}H_{28}N_6O_4Pd$

Anal. calcd., %	C, 57.62	H, 4.23	N, 12.60
Found, %	C, 57.70	H, 4.30	N, 12.58

IR (ν, cm^{-1}): 1627 (CH=N), 1597, 1538, 1520, 1497, 1462, 1443, 1377, 1333, 1186, 1146, 1120, 1088, 1013, 915, 889, 820, 752, 695, 662, 600. ^{1}H NMR (DMSO-d_6; δ, ppm): 2.21 (s, 3H, CH_3), 4.59 (s, 2H, CH_2), 6.10 (d, J = 3.0 Hz, 1H, H^3_{furyl}), 6.17 (t, J = 2.6 Hz, 1H, H^4_{furyl}), 7.25 (t, J = 7.2 Hz, 1H, H^4_{phenyl}), 7.41 (t, J = 7.8 Hz, 2H, H^3 and H^5_{phenyl}), 7.57–7.60 (m, 3H, H^2 and H^6_{phenyl}, H^5_{furyl}), 7.80 (s, 1H, CH=N).

Elemental analysis to C, H, N was carried out on a Carlo Erba Instruments TCM 480 instrument. Analysis to metal was conducted by the gravimetric method. Melting points were measured on a Kofler stage. The IR spectra of the samples were recorded on a Varian 3100-FTIR Excalibur instrument in a range of 4000–400 cm^{-1} using the attenuated total reflectance (ATR) method. ^{1}H NMR spectra were detected on a Varian Unity-300 instrument (300 MHz) in DMSO-d_6. The ^{1}H chemical shifts are presented relative to residual signals of the deuterated solvent.

The specific magnetic susceptibility was determined by the relative Faraday method at room temperature using $Hg[Co(CNS)_4]$ as the standard for calibration.

Absorption spectra were recorded in 2.0×10^{-5} M solutions on an Agilent 8453 spectrophotometer. Photoluminescence (PL) spectra were measured in 5.0×10^{-6} M solutions on a Varian Cary Eclipse fluorescence spectrophotometer. All spectra were detected for solutions in dichloromethane (CH_2Cl_2, high-purity grade for spectroscopy, Acros Organics) at room temperature. The fluorescence quantum yield was determined relative to the standard (3-methoxy-7*H*-benz[de]anthracen-7-one) in toluene (Φ_{Fl} = 0.1 for excitation at 365 nm) [34].

Quantum-chemical calculations were performed in terms of the density functional theory (DFT) using the Perdew–Burke–Ernzerhof exchange correlation functional PBE0 [35, 36] and Dunning's correlation-consistent polarized split valence basis set cc-pVDZ [37]. The Gaussian'03 program was used [38]. The geometry of molecules was optimized without symmetry restraints, and minima of the potential energy surface were characterized by the absence of imaginary frequencies of calculated normal vibrations. The influence of the medium was taken into account in terms of the polarizable continuum model [39] using parameters for the solvent (CH_2Cl_2).

XRD. Diffraction reflections intensities for compounds **Ia** and **Ic** were measured on the Belok/XSA diffraction beamline of the National Research Center Kurchatov Institute using a Rayonix Sx165 two-coordinate CCD detector (T = 100 K, φ scan mode with an increment of 1.0°) [40, 41]. Experimental data were processed using the XDS program, and an X-ray absorption correction was applied using the XSCALE program [42]. The main crystallographic data and refinement parameters are given in Table 1.

The structures were solved by direct methods and refined by full-matrix least squares for F^2 in the anisotropic approximation for non-hydrogen atoms. The positions of other hydrogen atoms in compounds **Ia** and **Ic** were calculated geometrically and included into refinement with fixed parameters (riding model) and isotropic displacement parameters (U_{iso}(H) = 1.5U_{eq}(C) for CH_3 groups and U_{iso}(H) = 1.2U_{eq}(C) for other groups). All calculations were performed using the SHELXTL software [43].

The structures of complexes **Ia** and **Ic** were deposited with the Cambridge Crystallographic Data Centre (CIF files CCDC nos. 2177619 and 2177622, respectively; deposit@ccdc.cam.ac.uk or http://www.ccdc.cam.ac.uk).

Antibacterial activity was evaluated using *Staphylococcus aureus* 6538 P and *Escherichia coli* F 50 strains (field isolates from the collection of the Rostov-on-Don Oblast Veterinary Laboratory) using the agar diffusion method [44, 45]. Furazolidone served as the reference product. The antibacterial activity level was determined from the sizes of the growth inhibition zones.

The fungistatic activity of the new substances was studied on the fungal culture of the *Penicillium* genus, *Penicillium italicum* Wehmer species (1894) (field isolate) from the Collection of Micromycetes of the Laboratory of Mycotoxicology at the North Caucasian Zonal Scientific Research Veterinary Institute using a known procedure [44]. Fundazole served as the reference substance.

The protistocidal activity was studied on protists of the *Colpoda steinii* species (field isolate) from the col-

Table 1. Crystallographic data and structure refinement parameters for complexes **Ia** and **Ic**

Parameter	Value	
	Ia	**Ic**
Empirical formula	$C_{32}H_{28}N_6O_4Cu$	$C_{32}H_{28}N_6O_4Co$
FW	624.14	619.53
Temperature, K	100(2)	100(2)
Crystal system	Monoclinic	Triclinic
Space group	$C2/c$	$P\bar{1}$
a, Å	17.207(3)	8.8100(18)
b, Å	16.484(3)	11.480(2)
c, Å	21.443(4)	14.480(3)
α, deg	90	105.28(3)
β, deg	104.24(3)	97.16(3)
γ, deg	90	91.62(3)
Volume, Å^3	5895(2)	1398.8(5)
Z	8	2
ρ_{calc}, g/cm^3	1.411	1.476
μ, mm^{-1}	0.888	0.895
F(000)	2600.0	646.0
Crystal size, mm	0.15 × 0.1 × 0.1	0.1 × 0.05 × 0.05
Wavelength	λ = 0.7454	λ = 0.79312
Range over 2θ, deg	from 5 to 62.002	from 5.768 to 76.97
Index range	$-23 \le h \le 23$, $-22 \le k \le 22$, $-28 \le l \le 29$	$-13 \le h \le 13$, $-14 \le k \le 14$, $-22 \le l \le 18$
Collected reflections	32246	19362
Independent reflections (R_{int}, R_{sigma})	7998 (0.0355, 0.0291)	8764 (0.0522, 0.0641)
Data/restraints/parameters	7998/0/390	8764/0/390
GOOF	1.050	1.099
R factors ($I > 2\sigma(I)$)	$R_1 = 0.040$, $wR_2 = 0.113$	$R_1 = 0.044$, $wR_2 = 0.127$
R factors (all data)	$R_1 = 0.0511$, $wR_2 = 0.1205$	$R_1 = 0.0560$, $wR_2 = 0.1317$
Electron density (max/min), e Å^{-3}	0.95/–0.99	0.55/–0.81

lection of the Laboratory of Parasitology at the North Caucasian Zonal Scientific Research Veterinary Institute. The protistocidal activity was studied by the serial dilution method using a described procedure [44–46] on the protist culture of the *Colpoda steinii* species. Chloroquine served as the reference substance.

RESULTS AND DISCUSSION

Continuing the studies [1–10, 28–31] of the structures and properties of new chelates containing the pyrazole fragment, we synthesized HL and related metal complexes ML_2 (M = Cu, Ni, Co, Zn, Pd) (Scheme 1).

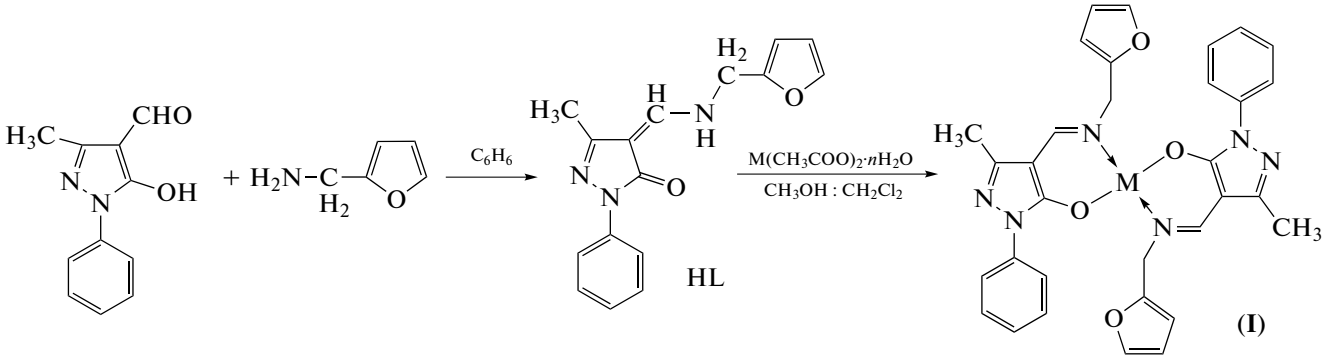

M = Cu (**Ia**), Ni (**Ib**), Co (**Ic**), Zn (**Id**), Pd (**Ie**)

Scheme 1.

The structure of HL was solved according to the data of elemental analysis, IR spectroscopy, ^{1}H NMR, and quantum-chemical calculations. Compounds of this type can exist in different tautomeric forms and as *E*,*Z* isomers [25, 27, 47]. The amino derivatives of aldehydes and pyrazol-5-one ketones can exist in solutions as both the keto-amine (A) and enol-amine (B) forms with a possibility of tautomeric transitions to occur. The quantum-chemical DFT calculations of HL showed that keto-amine form A is preferable in both the gas phase and CH_2Cl_2 solution (Scheme 2). The calculated energy of the tautomeric transition for HL in the gas phase turned out to be very close to the value Δ = 6.99 kcal/mol (B3LYP/6-31G(d,p)) obtained for similar N,N,O-tridentate tosylamino-functionalized pyrazole-containing Schiff base [3].

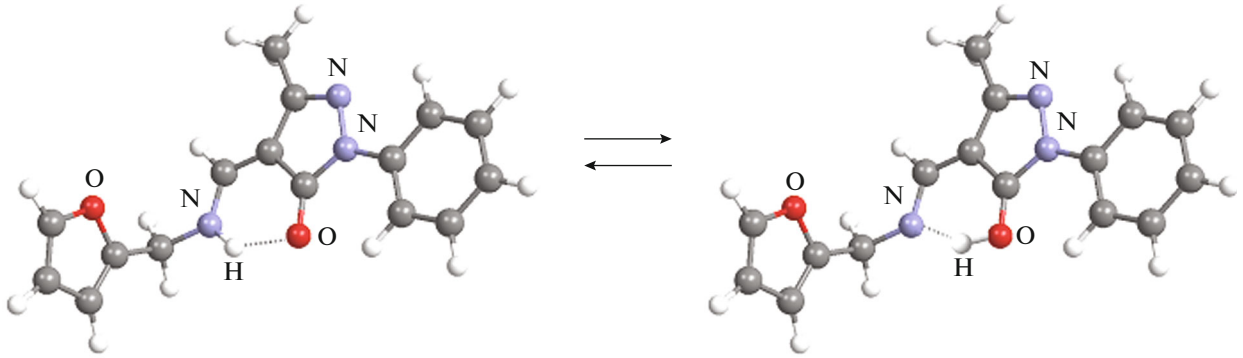

A
0 (g, CH_2Cl_2) kcal/mol

B
6.3 (g), 9.7 (CH_2Cl_2) kcal/mol

Scheme 2.

The keto-amine form of HL is also confirmed by the IR spectroscopy and ^{1}H NMR data for this compound. The IR spectrum of HL exhibits intense absorption bands at 3219 cm^{-1} ν(NH) and 1681 and 1667 cm^{-1} ν(C=O) corresponding to vibrations of the vinylogous amide group C(=O)–CH=NR [9]. The ^{1}H NMR spectrum of HL contains signals of protons at 8.10 ppm (CH–NH) and 9.74–9.78 ppm (CH–NH).

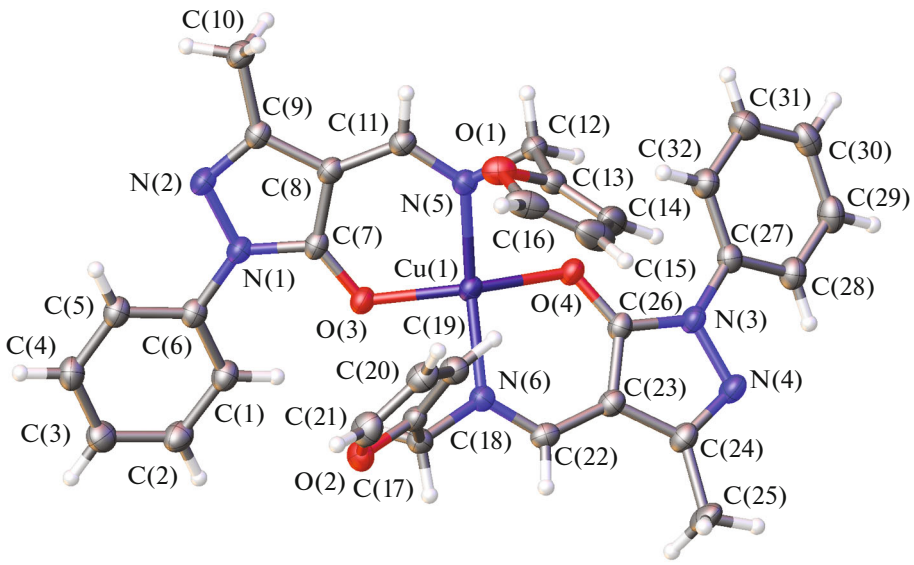

Fig. 1. Molecular structure of complex **Ia** in the representation of atoms by atomic shift ellipsoids at 50% probability level.

According to the elemental analysis data, metal complexes **Ia**–**Ie** have the composition ML_2. In the IR spectra of complexes **Ia**–**Ie**, the νNH and νC=O absorption bands of HL disappear and intense ν(CH=N) absorption bands appear in ranges of 1626 cm^{-1} (M = Cu, **Ia**), 1633 cm^{-1} (M = Ni, **Ib**), 1621 cm^{-1} (M = Co, **Ic**), 1620 cm^{-1} (M = Zn, **Id**), and 1627 cm^{-1} (M = Pd, **Ie**) indicating the formation of chelate structures **I** with HL [4, 9, 25–27, 48] and the transformation of the keto-amine form of the ligand (A) into the deprotonated enolate-imine form upon the coordination with the metal ions. This is confirmed by the ^{1}H NMR spectra of the Zn (**Id**) and Pd (**Ie**) complexes in which the CH–NH and NH–CH signals of the HL protons disappear and the signals of the CH=N group appear at 8.36 and 7.80 ppm, respectively.

Complexes **Ia**–**Ic** are paramagnetic. The values of μ_{eff} are 2.10 μ_B (M = Cu), 3.12 μ_B (M = Ni), and 4.26 μ_B (M = Co) at 294 K and remain unchanged with decreasing temperature, which indicates their mononuclear structure.

The final conclusion about the structures of complexes **Ia** and **Ic** was made on the basis of the XRD data. Their molecular structures are shown in Figs. 1 and 2, respectively. Selected geometric parameters for complexes **Ia** and **Ic** are listed in Table 2.

Complex **Ia** (Fig. 1) crystallizes in the monoclinic space group *C*2/*c*. Two deprotonated ligands HL are coordinated via the chelate mode to the copper(II) ion by the N atoms of the azomethine bond and the O atom of the aldehyde component of the ligand to form six-membered chelate cycles. The geometry of the copper(II) ion environment corresponds to a distorted planar square. Both six-membered chelate rings are nearly coplanar to the five-membered pyrazole rings (the angles between the planes are 1.138(5)° and 1.740(5)°). In the pyrazole fragments of the ligands, the phenyl rings are turned toward different directions relative to the five-membered pyrazole heterocycles by 19.152(7)° and 20.152(7)°. The five-membered furyl fragments form substantially different angles with the six-membered chelate cycles: 75.508(5)° and 85.316(5)°. The obtained distances Cu...O (1.9312(14), 1.9459(13) Å) and Cu...N (1.9762(16), 1.9706(16) Å) are close to analogous bond lengths in the structurally similar copper(II) complex with 4-[(benzylamino)phenylmethylene]-5-methyl-2-phenylpyrazol-3-one ligands (Cu...O

Table 2. Bond lengths and bond angles for complexes **Ia** and **Ic**

M = Cu, Co	**Ia**	**Ic**
	Bond lengths, Å	
M–O(3)	1.9312(14)	1.9538(13)
M–O(4)	1.9459(13)	1.9389(13)
M–N(5)	1.9762(16)	1.9900(14)
M–N(6)	1.9706(16)	1.9898(15)
	Angle, deg	
O(3)MO(4)	150.113(57)	107.368(55)
N(5)MN(6)	151.173(66)	120.396(55)
N(5)MO(4)	91.181(59)	117.748(57)
O(4)MN(6)	96.621(61)	98.673(57)
N(5)MO(3)	95.726(60)	100.269(54)
O(3)MN(6)	91.203(59)	112.309(52)

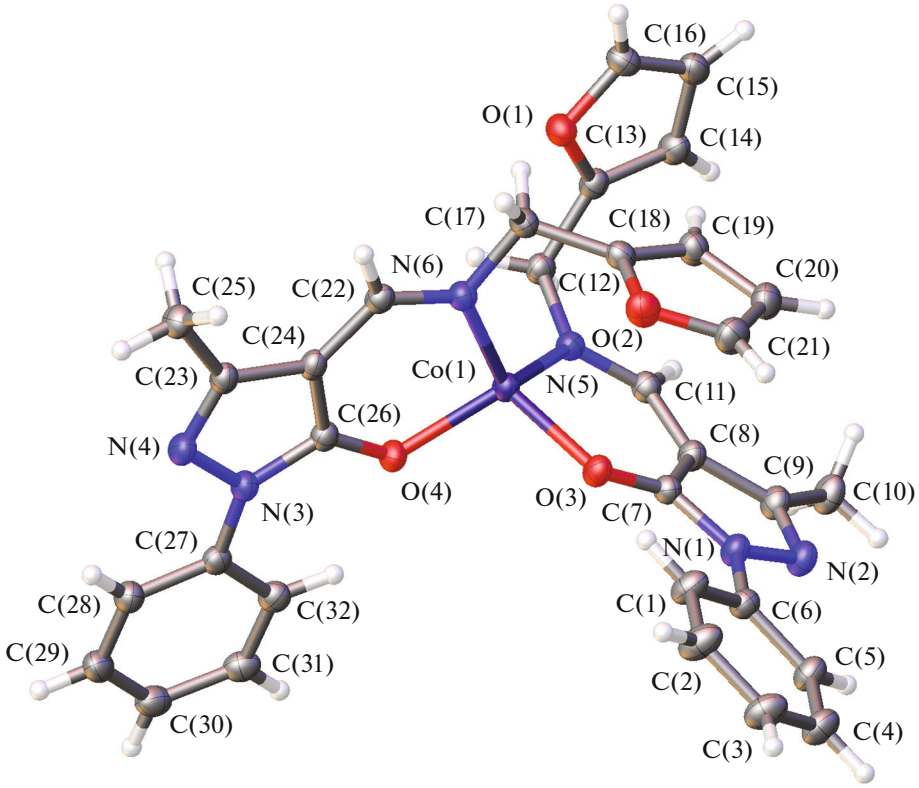

Fig. 2. Molecular structure of complex **Ic** in the representation of atoms by atomic shift ellipsoids at 50% probability level.

1.916(1), 1.922(1) Å and Cu...N 1.973(2), 1.984(2) Å, respectively [49]). No substantial hydrogen bonds or π interactions between adjacent molecules of the complex were found.

Complex **Ic** (Fig. 2) crystallizes in the triclinic space group $P\bar{1}$ and has the structure of the coordination node close to that in complex **Ia**. As for complex **Ia**, complex **Ic** exhibits the chelate coordination of two deprotonated ligands HL through the N and O atoms of the amine and aldehyde fragments of the ligand with the formation of six-membered chelate cycles. Based on the angles between the bonds (Table 2), we can say that complex **Ic** is characterized by the formation of a distorted tetrahedral coordination environment around the cobalt(II) ion. The angles between the planes of the six-membered chelate rings and pyrazole heterocycle are close and equal to 4.745(5)° and 4.648(5)°, whereas the turning angles of the phenyl substituents relative to the five-membered pyrazole rings are smaller than those in complex **Ia** and are equal to 6.845(5)° and 11.048(6)°, respectively. The five-membered furyl heterocycles form with the six-membered chelate rings angles of 87.504(5)° and 82.16(5)°, which do not differ strongly from the angles in complex **Ia**. Both the angles between the bonds and the bond lengths in complex **Ic** are close to the values obtained for analogous cobalt(II) complex with 4-[(benzylamino)phenylmethylene]-5-methyl-2-phenylpyrazol-3-one ligands (Co...O 1.925(2), 1.931(2) Å and Co...N 1.993(2), 1.996(2) Å) [50]. As for complex **Ia**, no hydrogen bonds or π interactions between adjacent molecules of complex **Ic** were observed.

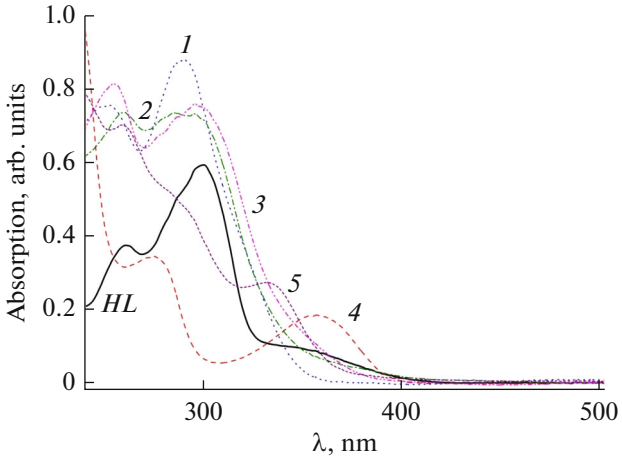

Fig. 3. Absorption spectra of solutions of HL and complexes (*1*) **Ia**, (*2*) **Ib**, (*3*) **Ic**, (*4*) **Id**, and (*5*) **Ie** in CH_2Cl_2 ($c = 2 \times 10^{-5}$ M, $l = 1$ cm, $T = 293$ K).

The absorption spectra of compounds HL and **Ia**–**Ie** in CH_2Cl_2 at room temperature are shown in Fig. 3. The absorption spectra of ligand HL in a spectral

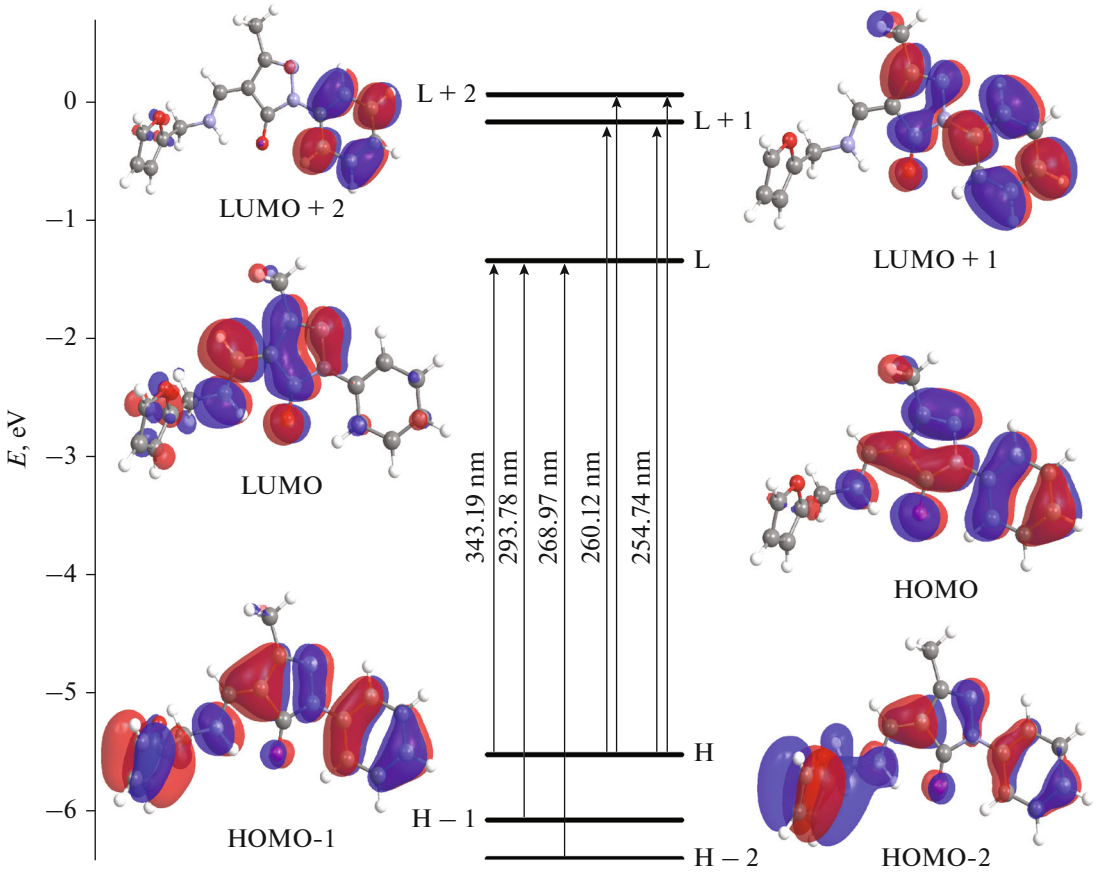

Fig. 4. Energy diagram, view of the isosurfaces of the frontier MOs, and main electron transitions for HL.

range of 240–500 nm are characterized by three absorption bands with maxima at 261, 300, and 357 nm, respectively (Fig. 3). The absorption bands of HL were assigned by the TD-DFT calculations for the optimized structure of the compound taking into account solvation effects. The characteristics of singlet-singlet electron transitions were calculated for HL, and they were assigned for the observed bands in the experimental absorption spectrum. The calculated values of the absorption band maxima (λ_{theor}) caused by the main electron singlet-singlet transitions between frontier molecular orbitals (MO), the corresponding oscillator forces for these transitions, and experimental absorption band maxima (λ_{exp}) for HL are given in Table 3. The energy diagram, view of the isosurfaces of the frontier MO, and main electron transitions for HL are shown in Fig. 4.

According to the calculations, the long-wavelength absorption band of HL with a low intensity at 357 nm can be assigned to the electron transition HOMO → LUMO with the low oscillator force $f = 0.02$. This transition represents the intraligand π–π* charge transfer from the phenyl ring to the pyrazole fragment of the molecule. The main absorption band maximum in the spectrum of HL at 300 nm is caused by one very strong transition HOMO-1 → LUMO and a weaker transition HOMO-4 → LUMO. The first transition is the intraligand π–π* charge transfer from the phenyl ring to the furan fragment of the molecule. The absorption band at 261 nm in the absorption spectrum

Table 3. Calculated (λ_{theor}) and experimental (λ_{exp}) absorption band maxima, contributions of particular electron transitions, and oscillator forces *f* for HL obtained from the TD-DFT calculations

λ_{exp}, nm	λ_{theor}, nm	Electron transitions (contributions, %)	*f*
357	343.19	HOMO → LUMO (94%)	0.02
300	293.78	HOMO-1→ LUMO (77%)	0.35
	284.00	HOMO-4 → LUMO (92%)	0.04
261	268.97	HOMO-2 → LUMO (76%)	0.33
	260.12	HOMO → LUMO+1 (50%) HOMO → LUMO+2 (22%)	0.17
	254.74	HOMO → LUMO+2 (44%) HOMO → LUMO+1 (42%)	0.25

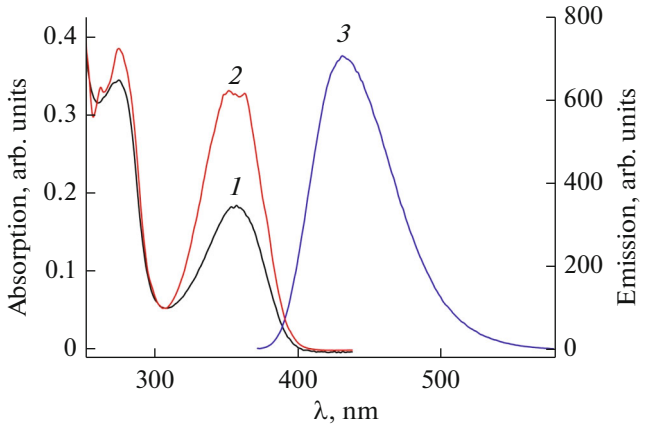

Fig. 5. Absorption spectra of complex **Id** (*1*) and its PL excitation (*2*, λ_{abs} = 450 nm) and PL emission (*3*, λ_{exc} = 365 nm) spectra in CH_2Cl_2 at room temperature.

of HL is characterized by several electron transitions between HOMO and LUMO + 1, LUMO + 2, i.e., intraligand π–π* charge transfer from the pyrazole fragment of the molecule to the phenyl ring.

The metal nature exerts a substantial effect on the absorption properties of complexes **Ia**–**Ie**. The absorption spectra of coordination compounds **Ia**–**Ic** based on copper(II), nickel(II), and cobalt(II) are characterized by two absorption bands with maxima at 253–260 nm (ε = 36820–40730 L mol^{-1} cm^{-1}) and at 291–296 nm (ε = 36750–44320 L mol^{-1} cm^{-1}), whose intensity is ~2 times higher than that of ligand HL (Fig. 3). Unlike ligand HL, zinc complex **Id** is characterized by two absorption bands with maxima at 275 nm (ε = 17240 L mol^{-1} cm^{-1}) and 357 nm (ε = 9250 L mol^{-1} cm^{-1}). The doubled intensity of the long-wavelength absorption band of zinc complex **Id** compared to the corresponding absorption of the ligand is consistent with its structure ZnL_2. The long-wavelength absorption band maximum of palladium complex **Ie** exhibits the hypsochromic shift by 25 nm compared to the zinc complex (Fig. 3).

Zinc complex **Id** manifests the PL properties in CH_2Cl_2 solutions at room temperature demonstrating blue emission with the emission band maximum at 431 nm (Fig. 5). The fluorescence quantum yield is 0.29. A comparative analysis of the absorption spectrum of compound **Id** with the excitation spectrum of observed fluorescence demonstrates their good coincidence indicating that the observed PL belongs to the coordination compound. No PL was observed for ligand HL and coordination compounds **Ia**–**Ic** and **Ie** under similar conditions. Thus, the metal nature exerts a substantial effect on the fluorescence properties of the synthesized complexes.

The synthesized enamine HL and *d*-metal complexes **Ia**–**Ie** were studied for antibacterial, protistocidal, and fungistatic activities. Enamine HL and all complexes **Ia**–**Ie** were found to have no fungistatic activity against *Penicillium italicum* and no antibacterial activity against *Staphylococcus aureus* and *Escherichia coli*.

The study of the protistocidal properties showed that enamine HL and the nickel (**Ib**) and cobalt (**Ic**) complexes manifested no protistocidal activity and the activity of the copper (**Ia**) and zinc (**Id**) complexes against *Colpoda steinii* was 32 times weaker than the activity of chloroquine.

ACKNOWLEDGMENTS

The work was carried out using equipment of the Center for Collective Use "Molecular Spectroscopy" of the Southern Federal University.

FUNDING

The research was carried out with the financial support of the Ministry of Science and Higher Education of the Russian Federation (state assignment in the field of scientific activity 2023, no. FENW-2023-0014).

CONFLICT OF INTEREST

The authors declare that they have no conflicts of interest.

REFERENCES

1. Uraev, A.I., Nefedov, S.E., Lyssenko, K.A., et al., *Polyhedron*, 2020, vol. 188, p. 114623. https://doi.org/10.1016/j.poly.2020.114623
2. Garnovskii, D.A., Vlasenko, V.G., Lyssenko, K.A., et al., *Polyhedron*, 2020, vol. 190, p. 114763. https://doi.org/10.1016/j.poly.2020.114763
3. Garnovskii, D.A., Vlasenko, V.G., Aleksandrov, G.G., et al., *Russ. J. Coord. Chem.*, 2018, vol. 44, p. 596. https://doi.org/10.1134/S0132344X18050031
4. Uraev, A.I., Lyssenko, K.A., Vlasenko, V.G., et al., *Polyhedron*, 2018, vol. 146, p. 1. https://doi.org/10.1016/j.poly.2018.02.018
5. Uraev, A.I., Korobov, M.S., Popov, L.D., et al., *Russ. J. Gen. Chem.*, 2017, vol. 87, p. 252. https://doi.org/10.1134/S1070363217020165
6. Garnovskii, D.A., Aleksandrov, G.G., Makarova, N.I., et al., *Russ. J. Inorg. Chem.*, 2017, vol. 62, p. 1077. https://doi.org/10.1134/S0036023617080071
7. Garnovskii, D.A., Antsyshkina, A.S., Makarova, N.I., et al., *Russ. J. Inorg. Chem.*, 2015, vol. 60, no. 12, p. 1528. https://doi.org/10.1134/S0036023615120116
8. Burlov, A.S., Koshchienko, Y.V., Vlasenko, V.G., et al., *Russ. J. Gen. Chem.*, 2016, vol. 86, p. 2379. https://doi.org/10.1134/S1070363216100224
9. Burlov, A.S., Vlasenko, V.G., Lifintseva, T.V., et al., *Russ. J. Coord. Chem.*, 2020, vol. 46, p. 485. https://doi.org/10.1134/S1070328420070015
10. Vlasenko, V.G., Garnovskii, D.A., Aleksandrov, G.G., et al., *Polyhedron*, 2019, vol. 157, p. 6. https://doi.org/10.1016/j.poly.2018.09.065

11. Ying-Xin Zou, Xu Feng, Zhi-Yong Chu, et al., *Regul. Toxic. Pharm.*, 2019, vol. 103, p. 34. https://doi.org/10.1016/j.yrtph.2019.01.018
12. Micieli, G., Manzoni, G.C., Granella, F., et al., *Drug-Induced Headache. Advances in Applied Neurological Sciences*, Diene, H.C. and Wilkinson, M., Eds., Berlin: Springer, 1988, vol. 5. p. 20. https://doi.org/10.1007/978-3-642-73327-7_5
13. Ribeiro, N., Roy, S., Butenko, N., et al., *J. Inorg. Biochem.*, 2017, vol. 174, p. 63. https://doi.org/10.1016/j.jinorgbio.2017.05.011
14. Parvarinezhad, S., Salehi, M., Malekshah, R.E., et al., *Appl. Organomet. Chem.*, 2022, vol. 36, no. 3, p. e6563. https://doi.org/10.1002/aoc.6563
15. Venkateswarlu, K., Ganji, N., Daravath, S., et al., *Polyhedron*, 2019, vol. 171, p. 86. https://doi.org/10.1016/j.poly.2019.06.048
16. Poormohammadi, E.B., Behzad, M., Abbasi, Z., et al., *J. Mol. Struct.*, 2020, vol. 1205, p. 127603. https://doi.org/10.1016/j.molstruc.2019.127603
17. Jayarajan, R., Vasuki, G., and Rao, P.S., *Org. Chem. Int.*, 2010, vol. 2010, p. 648589. https://doi.org/10.1155/2010/648589
18. Burlov, A.S., Vlasenko, V.G., Dmitriev, A.V., et al., *Synth. Met.*, 2015, vol. 203, p. 156. https://doi.org/10.1016/j.synthmet.2015.02.028
19. Burlov, A.S., Koshchienko, Y.V., Makarova, N.I., et al., *Synth. Met.*, 2016, vol. 220, p. 543. https://doi.org/10.1016/j.synthmet.2016.06.025
20. Minkin, V.I., Tsivadze, A.Yu., Burlov, A.S., et al., Patent RF 2470025, *Byull. Izobret.*, 2012, no. 35.
21. Gusev, A.N., Kiskin, M.A., Braga, E.V., et al., *ACS Appl. Electron. Mater.*, 2021, vol. 3, no. 8, p. 3436. https://doi.org/10.1021/acsaelm.1c00402
22. Gusev, A.N., Braga, E.V., Kryukova, M.A., et al., *Russ. J. Coord. Chem.*, 2020, vol. 46, p. 251. https://doi.org/10.1134/S107032842004003X
23. Gusev, A.N., Kiskin, M.A., Braga, E.V., et al., *J. Phys. Chem. C*, 2012, vol. 123, no. 18, p. 11850. https://doi.org/10.1021/acs.jpcc.9b02171
24. Barkanov, A., Zakharova, A., Vlasova, T., et al., *J. Mater. Sci.*, 2022, vol. 57, p. 8393. https://doi.org/10.1007/s10853-021-06721-4
25. Marchetti, F., Pettinari, C., Di Nicola, C., et al., *Coord. Chem. Rev.*, 2019, vol. 401, p. 213069. https://doi.org/10.1016/j.ccr.2019.213069
26. Marchetti, F., Pettinari, C., and Pettinari, R., *Coord. Chem. Rev.*, 2005, vol. 249, p. 2909. https://doi.org/10.1016/j.ccr.2005.03.013
27. Marchetti, F., Pettinari, C., and Pettinari, R., *Coord. Chem. Rev.*, 2015, vol. 303, p. 1. https://doi.org/10.1016/j.ccr.2015.05.003
28. Uraev, A., Nivorozhkin, A., Bondarenko, G., et al., *Russ. Chem. Bull. Int. Ed.*, 2000, vol. 49, p. 1863. https://doi.org/10.1007/BF02494925
29. Uraev, A.I., Korshunov, O.Y., Nivorozhkin, A.L., et al., *Russ. J. Inorg. Chem.*, 2009, vol. 54, no. 4, p. 521. https://doi.org/10.1134/S0036023609040068
30. Nivorozhkin, A.L., Uraev, A.I., Bondarenko, G.I., et al., *Chem. Commun.*, 1997, no. 18, p. 1711. https://doi.org/10.1039/a704879c
31. Uraev, A.I., Nivorozhkin, A.L., Divaeva, L.N., et al., *Russ. Chem. Bull.*, 2003, vol. 52, no. 11, p. 2523. https://doi.org/10.1023/B:RUCB.0000012379.96546.bb
32. Porai-Koshits, B.A. and Kvitko, I.Ya., *Zh. Obshch. Khim.*, 1962, vol. 32, p. 4050.
33. Kvitko, I.Ya. and Porai-Koshits, B.A., *Zh. Org. Khim.*, 1964, vol. 34, no. 9, p. 3005.
34. Krasovitskii, B.M. and Bolotin, B.M., *Organicheskie luminofory* (Organic Luminophores), Moscow: Khimiya, 1984, p. 336.
35. Perdew, J.P., Burke, K., and Ernzerhof, M., *Phys. Rev. Lett.*, 1997, vol. 78, p. 1396. https://doi.org/10.1103/physrevlett.78.1396
36. Perdew, J.P., Ernzerhof, M., and Burke, K., *J. Chem. Phys.*, 1996, vol. 105, p. 9982. https://doi.org/10.1063/1.472933
37. Woon, D.E. and Dunning, T.H., *J. Chem. Phys.*, 1993, vol. 98, p. 1358. https://doi.org/10.1063/1.464303
38. Frisch, M.J., Trucks, G.W., Schlegel, H.B., et al., *Gaussian 03, Revision A.1*, Pittsburgh: Gaussian, Inc., 2003.
39. Tomasi, J., Mennucci, B., and Cammi, R., *Chem. Rev.*, 2005, vol. 105, p. 2999. https://doi.org/10.1021/cr9904009
40. Lazarenko, V.A., Dorovatovskii, P.V., Zubavichus, Y.V., et al., *Crystals*, 2017, vol. 7, no. 11, p. 325. https://doi.org/10.3390/cryst7110325
41. Svetogorov, R.D., Dorovatovskii, P.V., and Lazarenko, V.A., *Cryst. Res. Tech.*, 2020, vol. 55, no. 5, p. 1900184. https://doi.org/10.1002/crat.201900184
42. Kabsch, W., *Acta Crystallogr., Sect. D: Biol. Crystallogr.*, 2010, vol. 66, no. 2, p. 125. https://doi.org/10.1107/S0907444909047337
43. Sheldrick, G.M., *Acta Crystallogr., Sect. C: Struct. Chem.*, 2015, vol. 71, p. 3. https://doi.org/10.1107/S2053229614024218
44. Burlov, A.S., Vlasenko, V.G., Koshchienko, Yu.V., et al., *Polyhedron*, 2018, vol. 154, p. 65. https://doi.org/10.1016/j.poly.2018.07.034
45. Burlov, A.S., Vlasenko, V.G., Koshchienko, Yu.V., et al., *Polyhedron*, 2018, vol. 144, p. 249. https://doi.org/10.1016/j.poly.2018.01.020
46. Fetisov, L.N., Zubenko, A.A., Bodryakov, A.N., and Bodryakova, M.A., *Mezhdunar. parazitologicheskii simp. "Sovremennye problemy obshchei i chastnoi parazitologii"* (Intern. Parasitological Symp. "Modern Problems of General and Special Parasitology"), 2012, p. 70.
47. Minkin, V.I., Garnovskii, A.D., Elguero, J., et al., *Adv. Heterocycl. Chem.*, 2000, vol. 76, p. 157.
48. Chatziefthimiou, S.D., Lazarou, Y.G., Hadjoudis, E., et al., *J. Phys. Chem. B*, 2006, vol. 110, p. 23701. https://doi.org/10.1021/jp064110p
49. Feng Bao, Juan Feng, and Seik Weng Ng, *Acta Crystallogr., Sect. E: Struct. Rep. Online*, 2005, vol. 61, p. m2393. https://doi.org/10.1107/S1600536805033805
50. Rong-Ming Ma, Shao-Fa Sun, and Seik Weng Ng, *Acta Crystallogr., Sect. E: Struct. Rep. Online*, 2006, vol. 62, p. m2711. https://doi.org/10.1107/S1600536806038049

Translated by E. Yablonskaya